Theoretical Study of the Electronic Spectrum of Indium Arsenide

Antara Dutta, Dipankar Giri, and Kalyan Kumar Das*

Department of Chemistry, Physical Chemistry Section, Jadavpur University, Kolkata 700 032, India

Received: April 25, 2001; In Final Form: June 27, 2001

The electronic spectrum of the indium arsenide molecule is studied by using an ab initio based multireference singles and doubles configuration interaction (MRDCI) method. Relativistic effective core potentials (RECP) of In and As atoms are used in the calculations. Potential energy curves of 39 Λ-S states of InAs have been reported. There are at least 19 Λ-S states that are bound within 42 000 cm^{-1} of energy. Spectroscopic constants (T_e, r_e, and ω_e) of these states are estimated. The observed ω_e for the ground state of the molecule agrees very well with the computed value, while the calculated transition energy of the $^3\Pi$ excited state is underestimated. The ground-state dissociation energy (D_e) of InAs is calculated to be 1.31 eV, which is comparable to that of InP. In the spin−orbit treatment, all 22 Λ-S states that correlate with the lowest two dissociation limits are included. The computed zero-field splitting of the ground state of InAs agrees well with the observed value. Transition dipole moments of many transitions are computed. Transition probabilities of $A^3\Pi-X^3\Sigma^-$, $A^3\Pi-{}^3\Pi$, $^3\Sigma^+-{}^3\Pi$, $4^1\Sigma^+-{}^1\Sigma^+$, and $4^1\Sigma^+-2^1\Sigma^+$ transitions are comparatively high. In the spin−orbit level six transitions from the $A^3\Pi_{0^+}$ component, which survives the predissociation, are studied. The radiative lifetimes of excited states are also estimated. The spectroscopic properties of InAs have been compared with those of the isovalent InP and InSb molecules.

I. Introduction

In recent years,[1−33] there has been considerable interest to study the electronic spectrum of semiconductor clusters and small molecules of groups III and V. Experimental studies of these types of molecules are outnumbered by limited theoretical work. The simple diatomic molecules such as GaP, InP, GaAs, InAs, GaSb, InSb, etc., and their ionic and neutral clusters of different sizes are important materials because of their technological usefulness. Of these, molecules and clusters of gallium arsenide are most widely studied. An extensive work on GaAs clusters after generating supersonic molecular beams by laser vaporization of the pure crystals has been carried out by Smalley and co-workers.[1−6] The characterization of these molecular beams has been done by laser photoionization and time-of-flight mass spectrometric measurement. The resonant two-photon ionization spectroscopy for the electronic structure and spectroscopic properties of the jet-cooled GaAs molecule have been carried out by Lemire et al.[7] The $^3\Pi-X^3\Sigma^-$ band system located in the range 23 000−24 800 cm^{-1} has been observed. Photodissociations of $\Omega = 2, 1, 0^-$ components of the $A^3\Pi$ state for $v' \geq 1$ of GaAs have been observed, while the $A^3\Pi_{0^+}$ component of the molecule is found to be stable. Similar predissociations are expected for the isovalent molecules of group III−V elements. Small clusters of Ga and P have been characterized recently.[8] The negative ion zero-electron kinetic photodetachment spectroscopic technique has been applied by Neumark and co-workers[9−13] to probe the electronic states of the neutral group IV and group III−V clusters. These studies provide information about the low-lying electronic states to which dipole-forbidden or spin-forbidden transitions may take place. The infrared absorption spectra of the diatomic InX (X = P, As, Sb) molecules, which are prepared by laser-vaporization of their crystals in rare gases and condensed on the gold surface at 4K, have been observed by Li et al.[14] Similar studies for the gallium series have been made by these authors.[15] The zero-field splitting $[^3\Sigma^-(1X_2)-{}^3\Sigma^-(0^+X_1)]$ in the ground state of InAs has been found to be 119 cm^{-1}, estimated from a very weak absorption in argon matrix. The band at 180.6 cm^{-1} has been assigned to InAs, while the absorption at 176.9 cm^{-1} is for the triatomic $InAs_2$. The harmonic force constant for the InAs molecule has been also reported. In the high-frequency region of the infrared spectrum of InAs in argon matrix, two progressions of bands with (0, 0) located at 3542.8 and 3650.8 cm^{-1}, are observed. However, one set of bands with (0, 0) at 3645.0 cm^{-1} is reported in neon matrix. These are assigned to the vibrational progression of the low-lying $^3\Pi$ state. No other theoretical or experimental studies of InAs are available for verification of these spectra.

An extensive review on relativistic effects for molecules and clusters has been made by Balasubramanian.[16,17] Experimental and theoretical studies on diatomic molecules such as GaP, GaAs, InP, and InSb are relatively well known. However, theoretical studies on the InAs molecule are not attempted so far. Feng and Balasubramanian[18,19] have performed configuration interaction (CI) calculations on clusters such as In_3P_2 and In_2P_3 and triatomic molecules such as In_2P, InP_2, In_2P^+, and InP_2^+. Electronic states and their potential energy curves of the isovalent gallium series are also calculated by these authors.[20,21] Recently, ab initio CI calculations on diatomic molecules such as GaP, InP, GaAs, InSb, and GaSb have been performed in our laboratory.[22−26] Because the $A^3\Pi-X^3\Sigma^-$ band for the gas-phase GaAs molecule has been observed in high-resolution spectroscopic measurements, calculations of the transition properties of A−X for group III−V semiconductor molecules are subject of much discussions in recent years.[24,27−29] It would be interesting to compare the spectroscopic properties of InAs with those of isovalent InP and InSb molecules. Meier et al.[30] have studied the isovalent AlP by a large scale CI calculations. Other phosphides such as AsP and SbP have been theoretically studied by Toscano and Russo.[31] Additionally, local spin density calculations for clusters and small molecules such as Sb_2, Sb_4, CuIn, AgIn, CuGa, AgGa, etc. have been reported by Russo and co-workers.[32,33]

The present paper is an attempt, for the first time to report the electronic spectrum of InAs from ab initio based CI calculations using relativistic pseudopotentials of the constituting

* Author for correspondence; e-mail: kalyankd@hotmail.com; fax: 91-33-473-1484.

10.1021/jp0115695 CCC: $20.00
Published on Web 09/07/2001

atoms. Effects of the spin−orbit interactions on the potential energy curves and spectroscopic properties of the low-lying Λ-S states of the molecule are explored in detail. We also report transition probabilities of dipole-allowed transitions with a special emphasis on the $A^3\Pi-X^3\Sigma^-$ transition analogous to the observed transition of the isovalent GaAs molecule. The radiative lifetimes of excited states are also the subject of the present study.

II. Computational Details

Ab initio based CI calculations of molecules with a large number of electrons have now become feasible because of the development of pseudopotential methods that reduce the number of active electrons participating in the configuration space. The $4d^{10}5s^25p^1$ electrons of In and $3d^{10}4s^24p^3$ electrons of As are kept in the valence space, while the remaining inner electrons are replaced by the semi-core RECPs of the corresponding atoms. The effective core potentials of In are taken from La John et al.,[34] while those for As are obtained from Hurley et al.[35] The 3s3p4d primitive Gaussian basis sets of indium and arsenic, taken from La John et al.[34] and Hurley et al.,[35] respectively, are the starting basis sets in the present calculations. The basis sets of In are augmented with one diffuse s($\xi = 0.02$ a_0^{-2}) and p($\xi = 0.0145$ a_0^{-2}) function, which are taken from Balasubramanian.[36] Similarly, the atomic basis set for arsenic is extended by adding one diffuse s and p function, whose exponents of 0.012 and 0.015 a_0^{-2}, respectively, are taken from Buenker et al.[37] The final basis sets of both atoms are 4s4p4d type in the uncontracted form. Moreover, these basis sets are compatible with the corresponding effective core potentials.

Self-consistent-field molecular orbital (SCF-MO) calculations for the $...\sigma^2\pi^2\ ^3\Sigma^-$ ground state with 28 valence electrons are carried out at each internuclear distance of InAs. At least 60 bond distances are chosen from 3.0 to 15.0 a_0 of the potential curve. The SCF calculations generate 80 symmetry-adapted MOs that are used as one-electron functions in the CI calculations. All calculations have been carried out in the C_{2v} symmetry group. In the CI step, $4d^{10}$ electrons of In and $3d^{10}$ electrons of As are kept frozen as these electrons remain localized on the corresponding atoms. So, only eight electrons are allowed to excite for the generation of configurations. The MRDCI codes of Buenker and co-workers[38−43] are used throughout the calculations, which are done in two steps. In the first step, Λ-S states are obtained without any spin−orbit coupling but with all other relativistic effects through RECP, while the spin−orbit interactions are introduced in the second stage. The lowest eight roots are computed for singlet, triplet, and quintet spin multiplicities of a given Λ-S symmetry. A set of important reference configurations is chosen for the entire potential energy curve of each Λ-S symmetry. All single and double excitations are allowed from these reference configurations. The generated configuration-space becomes of the order of million. The sizes of the secular equations are efficiently reduced by using a perturbative selection procedure of Buenker and co-workers.[38,39] The configuration-selection threshold in the present calculations has been kept at 1 μhartree. The sums of the squares of coefficients of reference configurations for the lowest roots remain above 0.90. The energy-extrapolation technique has been employed to estimate energies at the unselected level of treatment. Effects of higher excitations are incorporated through Davidson correction[44,45] to obtain an accurate estimate of the full CI energy. The computations use Table CI algorithm of Buenker and co-workers.[43]

In the next step, the Λ-S CI wave functions are employed as basis for the inclusion of the spin−orbit coupling. The spin−orbit operators for In and As derived from RECPs by LaJohn et al.[34] and Hurley et al.,[35] respectively, are used in this study. The spin−orbit matrix elements between pairs of appropriately selected CI wave functions are computed by using the spin-projection method and Wigner−Eckart theorem. The Λ-S full-CI energies are kept in the diagonals of the Hamiltonian matrix. The dimensions of the secular equations in A_1, A_2, and B_1 representations of the C_{2v}^2 group are 42, 42, and 43, respectively. Energies and compositions of Ω states are obtained after solving these secular equations explicitly. In the present calculations, spin−orbit components of all 22 Λ-S states, which correlate with the lowest two dissociation limits of InAs, are included for the spin−orbit interactions.

Potential energy curves of both Λ-S and Ω states are separately fitted into polynomials that are subsequently used for solving one-dimensional nuclear Schrödinger equations.[46] Spectroscopic parameters of bound states are estimated from these results. The vibrational energies and wave functions are used for the calculations of transition moments for all possible dipole-allowed transitions. Einstein coefficients and radiative lifetimes are computed from transition probabilities of various pairs of vibrational states.

III. Results and Discussion

Λ-S Potential Energy Curves and Their Properties. The interaction of $(5s^25p^1)\ ^2P$ In with $(4s^24p^3)\ ^4S$ As in their ground states generates four Λ-S states of quintet and triplet spin multiplicities. Eighteen Λ-S triplet and singlet states correlate with the In(^{2}P)+As(^{2}D) dissociation limit. The next higher limit In(^{2}P)+As(^{2}P) correlates with 12 triplet and singlet Λ-S states of Σ^+, Σ^-, Π, and Δ symmetries. Neither of the excited states of the As atom in the above three limits has any Rydberg character.

The computed potential energy curves of all triplet and quintet states of InAs are shown in Figure 1a, while singlet-state curves are given in Figure 1b. There are at least 19 Λ-S bound states within 42 000 cm^{-1} of energy. Spectroscopic properties, namely, r_e, T_e, and ω_e of these states as obtained from the present MRDCI calculations are reported in Table 1. The most stable electronic state ($X^3\Sigma^-$) of InAs is obtained from the $...\sigma^2\sigma^{*2}\sigma'^2\pi^2$ configuration. In the Franck−Condon region, the σ orbital is mainly the s orbital localized on As. However, a weak bonding character with the p_z(In) atomic orbital is noted. The σ^* orbital is antibonding comprising s(In) and s, p_z(As) orbitals, while the next occupied σ' orbital is strongly bonding of s, p_z(In), and p_z(As) orbitals. The highest occupied π MO at the ground-state equilibrium distance is almost pure $p_{x,y}$ orbitals. The lowest unoccupied π^* MO is strongly antibonding consisting of $p_{x,y}$ orbitals of In and As. The equilibrium bond length and vibrational frequency of the ground-state InAs are 2.76 Å and 179 cm^{-1}, respectively. Li et al.[14] have assigned the 180.6 cm^{-1} absorption band to InAs and 176.9 cm^{-1} band to the ν_3 stetching mode of the triatomic In_2As. The harmonic force constant of InAs calculated from the observed data is reported to be 8.72×10^4 dyn/cm. Therefore, the agreement of the calculated vibrational frequency with this experimental result is very good. The ground-state dissociation energy (D_e) of InAs is estimated to be 1.31 eV from the MRDCI energy of the molecule at $r = 15$ a_0 without considering any d-electron correlation and spin−orbit interaction. Although there are no experimental or theoretical data available for comparison, we may expect that the observed value would be somewhat larger than the present value. Earlier calculations[25] on the isovalent InSb molecule at the same level have shown the discrepancy between the calculated and observed D_e value is about 0.23 eV. In general, some disagree-

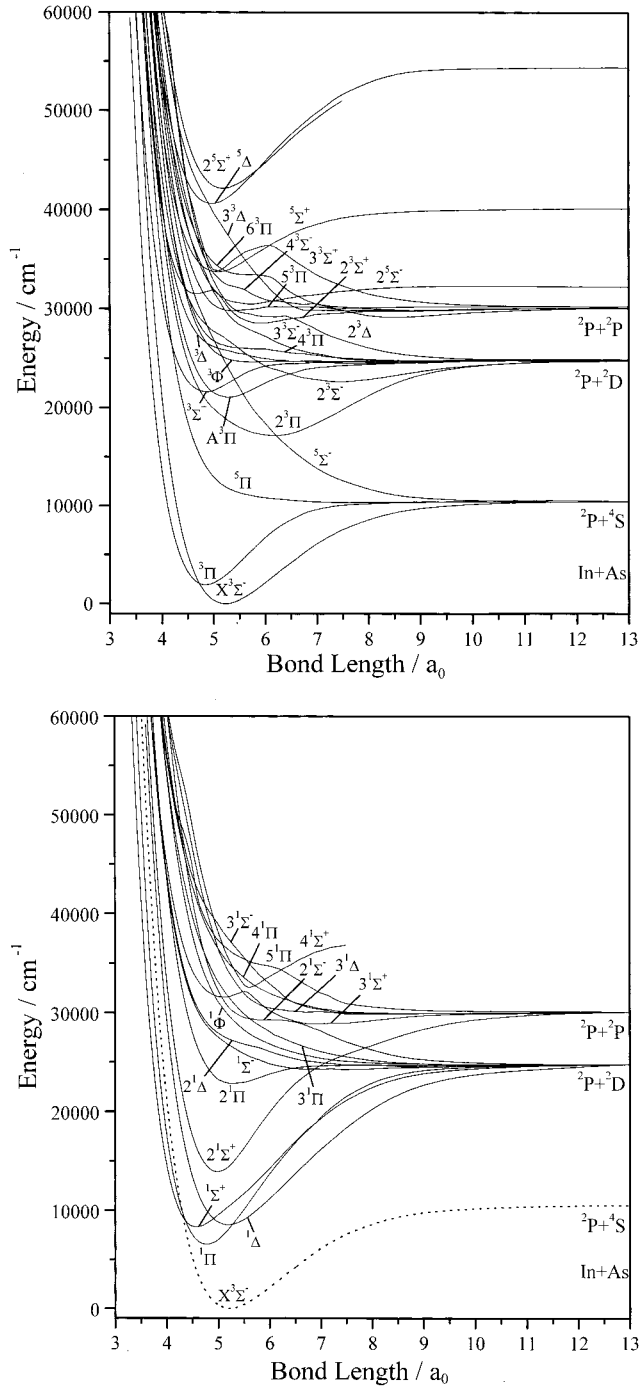

Figure 1. (a) Potential energy curves of triplet and quintet Λ-S states of InAs. (b) Potential energy curves of singlet Λ-S states of InAs (ground-state curve is shown by the dotted line for comparison).

ment is always expected because of the use of effective core potential approximation and the neglect of the d-correlation.

The $...\sigma^2\sigma^{*2}\sigma'^2\pi^2$ configuration is known to generate three Λ-S states: $X^3\Sigma^-$, $^1\Delta$, and $2^1\Sigma^+$, which are strongly bound. The $^1\Delta$ state correlates with ^{2}D, while $2^1\Sigma^+$ converges with the excited ^{2}P state of the As atom. The $2^1\Sigma^+$ state in the Franck−Condon region is found to be less pure than $^1\Delta$. The excited configuration $...\sigma^2\sigma^{*2}\pi^3\pi^*$ ($c^2 = 0.13$) and the closed shell configuration $...\sigma^2\sigma^{*2}\pi^4$ ($c^2 = 0.11$) contribute significantly in the formation of the $2^1\Sigma^+$ state at r_e. The spectroscopic parameters of the $^1\Delta$ state are found to be comparable to those of the ground state. This state is lying about 8530 cm^{-1} above the ground state. The adiabatic transition energy of the $2^1\Sigma^+$ state is computed to be 13 912 cm^{-1}. The shorter bond length and larger vibrational frequency of the $2^1\Sigma^+$ state are mainly due to a strong avoided crossing between the curves of $2^1\Sigma^+$ and $^1\Sigma^+$ states around 5.2 a_0. The CI wave functions of these two lowest $^1\Sigma^+$ states at different bond distances confirm this avoided crossing. At the bond length 6.0 a_0, the $^1\Sigma^+$ state is dominated by the $...\sigma^2\sigma^{*2}\sigma'^2\pi^2$ configuration, while the $2^1\Sigma^+$ state is characterized by the mixture of two important configurations such as $...\sigma^2\sigma^{*2}\pi^3\pi^*$ and $...\sigma^2\sigma^{*2}\pi$.[4]

TABLE 1: Spectroscopic Constants of the Λ-S States of InAs

state	T_e/cm^{-1}	r_e/Å	ω_e/cm^{-1}
$X^3\Sigma^-$	0	2.76	179(180.6)[a]
$^3\Pi$	1916 (3650)[a] [3000][b]	2.56	218
$^1\Pi$	6524	2.52	243
$^1\Sigma^+$	8285	2.42	244
$^1\Delta$	8530	2.75	189
$2^1\Sigma^+$	13912	2.63	253
$2^3\Pi$	17162	3.27	101
$A^3\Pi$	21076	2.79	163
$^3\Sigma^+$	21616	2.56	190
$2^3\Sigma^-$	22657	3.95	57
$2^1\Pi$	22801	2.81	143
$2^3\Sigma^+$(I)	28530	3.13	122
$3^1\Sigma^+$	28897	3.71	55
$2^5\Sigma^-$	30478	3.01	100
$2^3\Sigma^+$(II)	31470	2.46	227
$4^1\Sigma^+$	31495	2.67	162
$^5\Sigma^+$	33717	2.69	175
$^5\Delta$	40421	2.48	205
$2^5\Sigma^+$	42156	2.75	189

[a] Reference 14. [b] Vertical transition energy.

The first excited state of InAs is $^3\Pi$, which is mainly generated from a single excitation such as $\sigma' \rightarrow \pi$. Although the $...\sigma^2\sigma^{*2}\sigma'\pi^3$ configuration dominates in the description of the $^3\Pi$ state, a second configuration $...\sigma^2\sigma^{*2}\sigma'\pi^2\pi^*$, which is due to another single excitation $\sigma' \rightarrow \pi^*$, contributes significantly. According to our MRDCI results, the transition energy of the $^3\Pi$ state is found to be only 1916 cm^{-1}. However, Li et al.[14] have observed a Franck−Condon envelope with (0,0) band at 3650 cm^{-1} in argon matrices at 4 K and assigned to the vibrational progression of the lowest $^3\Pi$ state. There seems to be no other data available for further confirmation of this state. Earlier calculations[23,25] on isovalent molecules such as InP and InSb at the same level of approximation have shown that transition energies of their lowest $^3\Pi$ states are 2288 and 2654 cm^{-1}, respectively. Therefore, the calculated T_e of $^3\Pi$ for InAs is somewhat smaller than the expected value. The vertical transition energy of this state for InAs computed in this study is about 3000 cm^{-1}.

Table 1 shows that the second excited state of InAs is the singlet counterpart of $^3\Pi$. In the Franck−Condon region, the $^1\Pi$ state arises from the same excitation ($\sigma' \rightarrow \pi$) as that in $^3\Pi$. The $^1\Pi$ state has even shorter bond length ($r_e = 2.52$ Å) and longer vibrational frequency ($\omega_e = 243$ cm^{-1}) as compared with the corresponding triplet state. The calculated splitting [$\Delta E(^1\Pi - ^3\Pi)$] is about 4608 cm^{-1}. The $^1\Pi$ state dissociates into the excited (^{2}D) arsenic atom, whereas the $^3\Pi$ state correlates with the ground-state As(^{4}S). As a result, the $^1\Pi$ state is more strongly bound (binding energy = 2.26 eV) than its triplet counterpart. This is attributed to the increase in the delocalization of π molecular orbitals.

The MRDCI transition energy of the $^1\Sigma^+$ state is 8285 cm^{-1}. The In−As bond in this state is shorter than the ground-state bond by 0.34 Å. Similar to all other group III−V diatomics, the $^1\Sigma^+$ state of InAs has the shortest bond length among the low-lying states. The ω_e value of the $^1\Sigma^+$ state is about 65 cm^{-1} larger than that of the ground state. At r_e, the dominant closed

shell $...\sigma^2\sigma^{*2}\pi^4$ configuration has only 44% contribution. Three open shell configurations such as $...\sigma^2\sigma^{*2}\pi^3\pi^*$ ($c^2 = 0.29$), $...\sigma^2\sigma^*\sigma'\pi^4$ ($c^2 = 0.08$), and $...\sigma^2\sigma^{*2}\sigma'^2\pi^2$ ($c^2 = 0.02$) are also important to describe the $^1\Sigma^+$ state, which, however, undergoes an avoided crossing with the next higher $^1\Sigma^+$ state.

A broad and shallow potential well for the $2^3\Pi$ state has been shown in Figure 1a. This state is bound by about 7660 cm^{-1}, and the potential minimum is located around 6.2 a_0. The vibrational frequency at the minimum is only 101 cm^{-1}. The compositions of CI wave functions of the lowest two roots of the $^3B_1$ irreducible representation at different bond distances reveal the existence of a strong avoided crossing between $^3\Pi$ and $2^3\Pi$ state-curves. In the shorter bond length region, the $2^3\Pi$ state is represented mainly by $...\sigma^2\sigma^{*2}\sigma'\pi^2\pi^*$, while the contribution of this configuration diminishes with the increase in bond length and the $\sigma^2\sigma^{*2}\sigma'\pi^3$ configuration dominates. Therefore, the appearance of the potential minimum in the $2^3\Pi$ state-curve is purely due to such avoided crossing.

The $\sigma' \rightarrow \pi^*$ excitation generates four $^3\Pi$ states, of which $2^3\Pi$ and $3^3\Pi$ states are bound, while $4^3\Pi$ and $5^3\Pi$ states are repulsive in nature. We designate the $3^3\Pi$ state as $A^3\Pi$ in analogous with the A state of the GaAs molecule for which the $A^3\Pi-X\ ^3\Sigma^-$ band has been observed in the resonant two-photon ionization study. The $A^3\Pi$ state of InAs is comparatively weakly bound by about 3800 cm^{-1}. Its potential minimum is located at 2.79 Å with $\omega_e = 163$ cm^{-1}. It is expected to observe the $A^3\Pi-X^3\Sigma^-$ band for InAs in the region of 21 076 cm^{-1}. However, there are no experimental or other theoretical data available for confirmation. MRDCI calculations[23−25] of other isovalent indium molecules at the same level show that the transition energies for the $A^3\Pi$ state follow the expected trend T_e(InP) > T_e(InAs) > T_e(InSb). A similar trend has been observed for the corresponding gallium isomers. The $A^3\Pi$ state in the Franck−Condon region is represented by nearly a pure $...\sigma^2\sigma^{*2}\sigma'\pi^2\pi^*$ configuration ($c^2 = 0.79$). Because of the importance of the $A^3\Pi$ state with reference to its A−X transition, the spin−orbit effect on this state requires special attention.

A double excitation ($\sigma'^2 \rightarrow \pi\pi^*$) from the ground state generates the $^3\Sigma^+$ state, which is the next bound state of InAs. The CI wave functions of the $^3\Sigma^+$ state in the Franck−Condon region have shown that several other open shell configurations contribute to a smaller extent. The potential well of the $^3\Sigma^+$ state-curve is deep by 2770 cm^{-1} with a vibrational frequency of 190 cm^{-1}. The MRDCI calculations show that the In−As bond in this state is comparatively short ($r_e = 2.56$ Å). Potential energy curves of higher $^3\Sigma^+$ states, in particular $2^3\Sigma^+$ and $3^3\Sigma^+$, are shown in Figure 1a. Because of the strong avoided crossing between the curves of $2^3\Sigma^+$ and $3^3\Sigma^+$ states around 5.0a_0, there exists a double minima in the adiabatic curve of $2^3\Sigma^+$. The long-distant minimum at 3.13 Å is designated as the $2^3\Sigma^+$(I) state, which is bound by about 1300 cm^{-1}. The second minimum at 2.46 Å is denoted as $2^3\Sigma^+$(II). The estimated ω_e for the $2^3\Sigma^+$-(II) state curve is 227 cm^{-1}. The potential barrier from the short-distant minimum of the curve of $2^3\Sigma^+$ is only 400 cm^{-1}. The potential well of the $2^3\Sigma^+$(II) state consists of only one vibrational level. The compositions of CI wave functions of $2^3\Sigma^+$ and $3^3\Sigma^+$states at different bond distances confirm the avoided crossing that results in an apparent minimum in the adiabatic curve of the $3^3\Sigma^+$ state.

The potential energy curves of both $2^3\Sigma^-$ and $3^3\Sigma^-$ states correlate with the ^2D state of the arsenic atom. These two curves show a very strong avoided crossing. However, the $2^3\Sigma^-$ state has a shallow minimum near 3.95 Å and is bound by 2000 cm^{-1}. The transition energy of a strongly bound $2^1\Pi$ state is 22 801 cm^{-1}. At the equilibrium bond length, the state is represented by a dominant configuration $...\sigma^2\sigma^{*2}\sigma'\pi^2\pi^*$. It may be pointed out that the $\sigma' \rightarrow \pi^*$ excitation creates a total of 10 Λ-S states, of which $2^3\Pi$, $A^3\Pi$, $4^3\Pi$, and $5^3\Pi$ are already discussed. Of three $^1\Pi$ states, only $2^1\Pi$ is bound, while $3^1\Pi$ and $4^1\Pi$ states are repulsive in nature (see Figure 1b). The remaining three states such as $^1\Phi$, $^3\Phi$, and $^5\Pi$ are also found to be repulsive. The $^5\Pi$ state dissociates into the ground-state limit, while $^{1,3}\Phi$ states correlate with the next highest dissociation limit.

The characteristics of $3^1\Sigma^+$ and $4^1\Sigma^+$ states of InAs are interesting to note. As seen in Figure 1b, there is a sharp avoided crossing between these two states at $r = 5.6$ a_0. The shallow and weakly bound minimum at $r_e = 3.71$ Å is assigned to the $3^1\Sigma^+$ state, which correlates with the In(^{2}P)+As(^{2}P) limit. The CI wave functions at r_e show that the $3^1\Sigma^+$ state is generated mostly from a $\pi \rightarrow \pi^*$ excitation. The high-energy state is designated as $4^1\Sigma^+$. Because the interaction between $3^1\Sigma^+$ and $4^1\Sigma^+$ states is considerably small, we have fitted the diabatic curve of the $4^1\Sigma^+$ state for the estimation of spectroscopic constants. The $4^1\Sigma^+$ state is strongly bound and dissociates into the higher limit. The CI-estimated transition energy of this state at r_e is about 31 495 cm^{-1}. The In−As bond in this state is found to be shorter than the ground-state bond.

Although two low-lying $^5\Pi$ and $^5\Sigma^-$ states are repulsive correlating with the ground-state dissociation limit, some of the high-lying quintets are strongly bound and dissociate into higher limits. The present calculations show that the $2^5\Sigma^-$ state is bound by 1800 cm^{-1} with a longer equilibrium bond length and smaller vibrational frequency. The next most stable $^5\Sigma^+$ state is lying 33 717 cm^{-1} above the ground state, while the transition energy of the $2^5\Sigma^+$ state is 42 156 cm^{-1}. The r_e and ω_e values of both $^5\Sigma^+$ states are comparable with those of the ground state. Three configurations participate considerably for the description of both $^5\Sigma^+$ and $2^5\Sigma^+$ states in the Franck−Condon region. The remaining $^5\Delta$ state is strongly bound with $\omega_e = 205$ cm^{-1} and $T_e = 40\,421$ cm^{-1}. The bond length at the potential minimum of this state is shorter than that of the ground-state by about 0.28 Å. The state is dominantly represented by the $...\sigma^2\sigma^*\sigma'\pi^3\pi^*$ configuration.

The ground-state dissociation energy (D_e) of InAs computed from MRDCI calculations, which do not include any d-electron correlation and spin−orbit coupling, is found to be 1.31 eV. Although no experimental or other theoretical D_e of InAs is available for comparison, we may expect the present value to be underestimated to some extent. Earlier calculations on isovalent molecules of group III−V at the same level have shown that the calculated D_e values are expected to be smaller than the observed values by 0.3−0.5 eV. An improvement of D_e by about 0.2 eV for GaAs has been reported because of the d-electron correlation. In the present study, $4d^{10}$ and $3d^{10}$ electrons of In and As, respectively, are not correlated in the CI step. The present computations have been carried out with a sufficiently large basis set and small configuration-selection threshold. Therefore, we do not expect any significant improvement by increasing the size of the basis set and reducing the selection threshold further. However, some disagreement is expected because of the use of effective core potential approximations.

Potential Curves and Spectroscopic Constants of Ω States. The inclusion of the spin−orbit interaction in the Hamiltonian through the spin−orbit operators derived from RECPs results in splitting of Λ-S states into various Ω components. The mixing among Ω states of the same symmetry will change the electronic spectrum of the low-lying states of InAs. In the present

TABLE 2: Dissociation Correlation between Ω States and Atomic States of InAs

Ω state	atomic states In + As	relative energy/cm^{-1} expt.[a]	calc.
0^+, 0^-, 1(2), 2	$^2P_{1/2} + {}^4S_{3/2}$	0	0
$0^+(2)$, $0^-(2)$, 1(3), 2(2), 3	$^2P_{3/2} + {}^4S_{3/2}$	2213	2087
0^+, 0^-, 1(2), 2	$^2P_{1/2} + {}^2D_{3/2}$	10593	14077
0^+, 0^-, 1(2), 2(2), 3	$^2P_{1/2} + {}^2D_{5/2}$	10915	14461
$0^+(2)$, $0^-(2)$, 1(3), 2(2), 3	$^2P_{3/2} + {}^2D_{3/2}$	12806	16083
$0^+(2)$, $0^-(2)$, 1(4), 2(3), 3(2), 4	$^2P_{3/2} + {}^2D_{5/2}$	13128	16488

[a] Reference 47.

TABLE 3: Spectroscopic Constants of Ω States of InAs

state	T_e/cm^{-1}	r_e/Å	ω_e/cm^{-1}	composition at r_e
$X^3\Sigma^-_{0^+}$	0	2.764	180 (176.9)[a]	$X^3\Sigma^-$(98)
$X^3\Sigma^-_1$	92 (119)[a]	2.764	180	$^3\Sigma^-$(99)
$^3\Pi_2$	1480	2.565	218	$^3\Pi$(99)
$^3\Pi_1$	2014	2.564	219	$^3\Pi$(93)
$^3\Pi_{0^+}$	2680	2.570	216	$^3\Pi$(99)
$^3\Pi_{0^-}$	2688	2.569	217	$^3\Pi$(99)
$^1\Pi_1$	6790	2.526	243	$^1\Pi$(98), $^3\Pi$(2)
$^1\Sigma^+_{0^+}$	8531	2.431	241	$^1\Sigma^+$(99)
$^1\Delta_2$	8678	2.743	190	$^1\Delta$(99)
$2^1\Sigma^+_{0^+}$	14179	2.632	252	$2^1\Sigma^+$(99)
$2^3\Pi_2$	16984	3.275	102	$2^3\Pi$(60), $^5\Sigma^-$(38)
$2^3\Pi_1$	17324	3.227	121	$2^3\Pi$(84), $^5\Sigma^-$(11), $^1\Pi$(2), $^5\Pi$(1)
$2^3\Pi^-_0$	17675	3.227	97	$2^3\Pi$(94), $^5\Sigma^-$(2)
$2^3\Pi_{0^+}$	17819	3.225	110	$2^3\Pi$(99)
$A^3\Pi_{0^+}$	20918	2.845	148	$A^3\Pi$(95), $2^3\Pi$(4)
$^3\Sigma^+_1$	21567	2.593	203	$^3\Sigma^+$(73), $A^3\Pi$(22), $2^3\Sigma^-$(2), $2^3\Pi$(1)
$A^3\Pi_2$	21736	2.757	160	$A^3\Pi$(98)
$^3\Sigma^+_{0^-}$	21875	2.551	199	$^3\Sigma^+$(72), $A^3\Pi$(28)
$2^1\Pi_1$	23267	2.792	148	$2^1\Pi$(84), $A^3\Pi$(11), $^3\Sigma^+$(3)

[a] Reference 14.

calculations we have included all 22 Λ-S states which dissociate into the lowest two atomic limits for the spin−orbit interaction. These two lowest limits split into six asymptotes whose experimental and calculated energies are given in Table 2. Symmetries of all Ω states correlating with these asymptotes are also reported in the same table. The calculated spin−orbit splitting for the ^{2}P state of the indium atom agrees very well with the experimental value of 2213 cm^{-1}. The $^2D_{5/2}-{}^2D_{3/2}$ energy separation for As computed in this study differs from the observed value by less than 100 cm^{-1}. However, a large discrepancy of about 3500 cm^{-1} between ^{4}S and ^{2}D states of the arsenic atom persists, even after the inclusion of the spin−orbit coupling. Therefore, energies of all four limits arising from In(^{2}P)+As(^{2}D) are 3500 cm^{-1} higher than the observed values. It is expected that the ground-state dissociation energy is underestimated by this amount. The exact amount of such discrepancy cannot be confirmed because of the nonavailability of any experimental result. Earlier calculations[22−26] at the same level on diatomic molecules of group III−V show similar discrepancies.

Potential energy curves of all 51 Ω states are shown in Figures 2a−d, while the estimated spectroscopic constants and compositions of the bound Ω states are tabulated in Table 3. The zero-field splitting [$^3\Sigma^-(1X_2)-{}^3\Sigma^-(0^+X_1)$] for the ground-state InAs is computed to be 92 cm^{-1}, which agrees well with the observed value of 119 cm^{-1} in argon matrices. The calculations show that the X $^3\Sigma^-_{0^+}$ component lies below the other component $X^3\Sigma^-_1$. At the equilibrium bond distance, both the components remain almost pure $X^3\Sigma^-$, while at long distances the components of the repulsive $^5\Pi$ state begin to mix. There are no changes in r_e and ω_e values because of the spin−orbit coupling. The $X^3\Sigma^-_{0^+}$ state-curve in Figure 2a shows sharp avoided crossings with the curves of $^3\Pi_{0^+}$ and $^1\Sigma^+_{0^+}$ components at the shorter bond distances. Similar crossings are also noted in the curve of the other component X $^3\Sigma^-_1$ (see Figure 2c).

The spin−orbit components of the $^3\Pi$ state split as 2, 1, 0^+, and 0^- in the increasing order of energy. The largest spin−orbit splitting in this state has been computed to be 1208 cm^{-1}. At equilibrium bond lengths, these components are not strongly influenced by any nearby state and the spectroscopic constants remain almost unchanged. Analyzing the CI wave functions at the longer bond distances, it is seen that the components of $^5\Pi$ start mixing with those of the $^3\Pi$ state. However, several sharp avoided crossings are noted near the potential minima of $^3\Pi_{0^+}$ and $^3\Pi_1$ curves, while the curves of $^3\Pi_{0^-}$ and $^3\Pi_2$ components are not perturbed in the Franck−Condon region. We have estimated spectroscopic constants of these components by fitting the diabatic curves. The only component of $^1\Pi$ does not change much due to the spin−orbit coupling. The influence of the $^3\Pi_1$ component to the spectroscopic parameters of $^1\Pi_1$ is negligibly small because of the large energy gap of about 4780 cm^{-1} which prevents them to mix up significantly. Three successive singlet components such as $^1\Sigma^+_{0^+}$, $^1\Delta_2$, and $2^1\Sigma^+_{0^+}$ remain almost unperturbed by the spin−orbit interaction. The potential curve of $^1\Sigma^+_{0^+}$ in Figure 2a undergoes three sharp avoided crossings: first one with the $^3\Pi_{0^+}$ curve around 4.2 a_0 and the other two with the curves of $X^3\Sigma^-_{0^+}$ and $^5\Pi_{0^+}$ near 4.5 and 5.4 a_0, respectively. Another crossing with the $2^3\Pi_{0^+}$ state-curve is also noticeable at the longer bond distance. Similarly, the potential energy curve of $2^1\Sigma^+_{0^+}$ undergoes several avoided crossings. Figure 2d shows that there are two avoided crossings in the curve of $^1\Delta_2$, one with the curve of $^5\Pi_2$ and the other with that of $^5\Sigma^-_2$ around $r = 5.9$ and 6.7 a_0, respectively.

Three spin−orbit components (Ω = 2, 1, and 0^-) of the repulsive $^5\Sigma^-$ curve play an important role in determining the spectral behaviors of the Ω components of $2^3\Pi$ and $A^3\Pi$. It is already discussed that the appearance of the minimum in the potential curve of $2^3\Pi$ is due to an avoided crossing with the low-lying $^3\Pi$ state. With the inclusion of the spin−orbit interaction, the $2^3\Pi$ state splits as 2, 1, 0^-, and 0^+ in the ascending order of energy. The estimated spectroscopic constants of the diabatic potential curves of these components are shown in Table 3. Of the four components of the $A^3\Pi$ state, the components with Ω = 0^-, 1, and 2 interact with the corresponding components of the repulsive $^5\Sigma^-$ state, leading to the predissociations of these substates. The diabatic curves of $A^3\Pi_{0^-}$ and $A^3\Pi_1$ could not be fitted due to their complexiety in the Franck−Condon region. Therefore, only the $A^3\Pi_{0^+}$ component survives the predissociation, and the corresponding curve is less complicated. Two transitions such as $A^3\Pi_{0^+}-X^3\Sigma^-_{0^+}$ and $A^3\Pi_{0^+}-X^3\Sigma^-_1$ are important to study.

Transition Dipole Moments and Radiative Lifetimes of Excited States. There are no experimental or theoretical data available for transition moments of any dipole allowed transition in InAs. The radiative lifetime of any low-lying excited state is also not known so far. Transition probabilities of many electric dipole allowed transitions are computed in the present study. In the absence of the spin−orbit coupling, transitions involving $A^3\Pi$, $2^3\Pi$, $^3\Sigma^+$, $2^3\Sigma^+$(II), $2^1\Sigma^+$, $2^1\Pi$, and $4^1\Sigma^+$ states are considered. The computed transition moments of triplet−triplet and singlet−singlet transitions as a function of the internuclear distance are plotted in Figures 3a and 3b, respectively. These transition dipole moment functions are used for the estimation of transition probabilities, and hence the radiative lifetimes of the upper states at different vibrational levels. Two possible

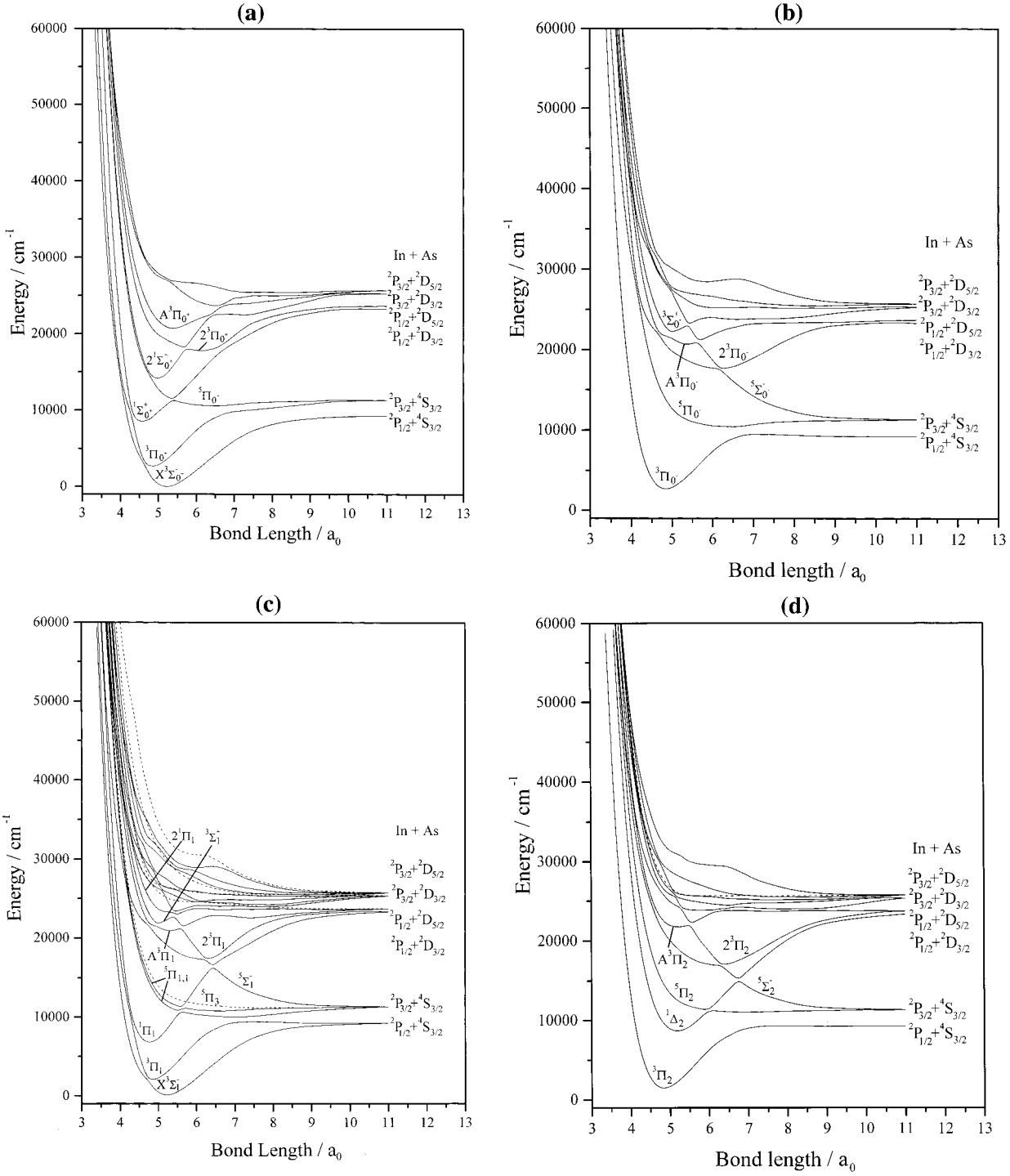

Figure 2. (a) Potential energy curves of low-lying $\Omega = 0^+$ states of InAs. (b) Potential energy curves of low-lying $\Omega = 0^-$ states of InAs. (c) Potential energy curves of low-lying $\Omega = 1$ and 3 states of InAs (the curve with dashed line is for $\Omega = 3$). (d) Potential energy curves of low-lying $\Omega = 2$ and 4 states of InAs (curves with dashed lines are for $\Omega = 4$).

dipole allowed transitions such as $A^3\Pi-X^3\Sigma^-$ and $A^3\Pi-{}^3\Pi$ are significant for group III−V diatomic molecules. The transition-moment curves for both transitions are very smooth with a maximum in the Franck−Condon region. In general, transition moments of the former transition are always much larger than the latter. As a result, the $A^3\Pi-X^3\Sigma^-$ transition is found to be stronger than the $A^3\Pi-{}^3\Pi$ transition. Table 4 shows the estimated radiative lifetimes of the upper triplet and singlet states at lowest three vibrational levels. The present calculations predict the total lifetime of the $A^3\Pi$ state at $v' = 0$ of the order of 250 ns. Although not yet observed, one would expect a strong A−X band around 21 000 cm^{-1}.

Of two symmetry allowed transitions involving $2^3\Pi$, the $2^3\Pi-X^3\Sigma^-$ transition is reasonably strong, while the $2^3\Pi-{}^3\Pi$ transition has a very low transition probability. As seen in Figure 3a, the largest value of the transition moment for the $2^3\Pi-X^3\Sigma^-$ transition is about 0.19 μa_0 at $r = 5.5$ a_0. The partial lifetime of the $2^3\Pi$ state is estimated to be 12.8 μs. Although the transition dipole moments for the $2^3\Pi-{}^3\Pi$ transition are calculated to be large throughout the potential curve, the Franck−Condon overlap terms are negligibly small because of the appearance of the potential minimum of the $2^3\Pi$ state at the longer bond distance region. At the lowest vibrational level, total radiative lifetime of the $2^3\Pi$ state remains at 12.8 μs. A

TABLE 4: Radiative Lifetimes of Some Excited Triplet and Singlet Λ-S States of InAs at Lowest Three Vibrational Levels[a]

transition	lifetimes(s) of the upper state $v'=0$	$v'=1$	$v'=2$	total lifetimes(s) of upper state at $v'=0$
$A^3\Pi-X\ ^3\Sigma^-$	2.66(−7)	2.73(−7)	2.80(−7)	
$A^3\Pi-{}^3\Pi$	4.02(−6)	3.25(−6)	2.79(−6)	$\tau(A^3\Pi) = 2.49(-7)$
$2^3\Pi-X^3\Sigma^-$	1.28(−5)	1.16(−5)	1.06(−5)	$\tau(2^3\Pi) = 1.28(-5)$
$^3\Sigma^+-{}^3\Pi$	1.12(−6)	1.14(−6)	1.16(−6)	$\tau(^3\Sigma^+) = 1.12(-6)$
$2^3\Sigma^+(II)-{}^3\Pi$	2.85(−7)	2.92(−7)	2.98(−7)	
$2^3\Sigma^+(II)-{}^3\Sigma^+$	5.95(−6)	5.80(−6)	5.66(−6)	
$2^3\Sigma^+(II)-A^3\Pi$	4.75(−3)	7.26(−4)	2.56(−4)	$\tau(2^3\Sigma^+(II)) = 2.72(-7)$
$2^1\Sigma^+-{}^1\Pi$	6.39(−6)	6.39(−6)	6.39(−6)	
$2^1\Sigma^+-{}^1\Sigma^+$	2.39(−5)	2.37(−5)	2.35(−5)	$\tau(2^1\Sigma^+) = 5.04(-6)$
$2^1\Pi-{}^1\Pi$	7.16(−7)	1.08(−6)	1.30(−6)	
$2^1\Pi-{}^1\Delta$	3.96(−6)	4.04(−6)	4.14(−6)	
$2^1\Pi-{}^1\Sigma^+$	9.64(−5)	1.00(−4)	1.08(−4)	
$2^1\Pi-2^1\Sigma^+$	1.26(−4)	1.22(−4)	1.19(−4)	$\tau(2^1\Pi) = 6.02(-7)$
$4^1\Sigma^+-{}^1\Sigma^+$	7.70(−8)	7.71(−8)	7.83(−8)	
$4^1\Sigma^+-2^1\Sigma^+$	4.89(−7)	4.74(−7)	4.70(−7)	
$4^1\Sigma^+-{}^1\Pi$	1.83(−5)	1.75(−5)	1.67(−5)	
$4^1\Sigma^+-2^1\Pi$	1.20(−5)	1.27(−5)	1.38(−5)	$\tau(4^1\Sigma^+) = 6.59(-8)$

[a] Values in the parentheses are the powers to the base 10.

reasonably strong $^3\Sigma^+-{}^3\Pi$ transition is expected to be observed around 19 700 cm^{-1}. The estimated lifetime of the $^3\Sigma^+$ state is about 1.12 μs.

Transitions from the $2^3\Sigma^+(I)$ state are found to be weak because of its shallow potential minimum at the longer bond distance. We have, therefore, estimated transition probabilities of transitions involving the $2^3\Sigma^+(II)$ state, which has a shorter r_e. The $2^3\Sigma^+(II)-{}^3\Pi$ transition is much stronger than the other two transitions such as $2^3\Sigma^+(II)-{}^3\Sigma^+$ and $2^3\Sigma^+(II)-A^3\Pi$. Although the transition moments for the $2^3\Sigma^+(II)-{}^3\Sigma^+$ transition in the Franck−Condon region are larger than those for the $2^3\Sigma^+(II)-A^3\Pi$ transition, the larger energy-difference makes the latter transition stronger. The overall radiative lifetime of the $2^3\Sigma^+$ state computed after adding all transition probabilities is found to be 227 ns.

Two transitions from the $2^1\Sigma^+$ state have been studied here. The transition-moment curves of both transitions, namely, $2^1\Sigma^+-{}^1\Pi$ and $2^1\Sigma^+-{}^1\Sigma^+$ show maxima around 5.0 a_0 (see Figure 3b). However, the transition dipole moment of the latter transition falls rapidly with the bond distance. Our calculations predict the former transition to be stronger than the latter. Combining these two transitions, the radiative lifetime of the $2^1\Sigma^+$ state is found to be 5.04 μs. The $2^1\Pi$ state involves four possible transitions: $2^1\Pi-{}^1\Pi$, $2^1\Pi-{}^1\Delta$, $2^1\Pi-{}^1\Sigma^+$, and $2^1\Pi-2^1\Sigma^+$. The transition dipole moments for the $2^1\Pi-{}^1\Pi$ transition are comparatively large, and hence this transition is stronger than the remaining three transitions. The transition-moment function for the $2^1\Pi-{}^1\Pi$ transition shows a maximum around 6.0 a_0. Both $2^1\Pi-{}^1\Sigma^+$ and $2^1\Pi-2^1\Sigma^+$ transitions are comparatively weak. The estimated lifetime of the $2^1\Pi$ state is about 0.6 μs. Four symmetry-allowed transitions are expected to take place from $4^1\Sigma^+$. The parallel transitions, namely, $4^1\Sigma^+-{}^1\Sigma^+$ and $4^1\Sigma^+-2^1\Sigma^+$, have strong transition probabilities, while perpendicular transitions are weak. The $4^1\Sigma^+-{}^1\Sigma^+$ transition should be observed around 23 200 cm^{-1}. Summing up transition probabilities of these four transitions, the total radiative lifetime of the $4^1\Sigma^+$ state is estimated to be only 66 ns.

The A−X transition draws more attention for group III−V diatomic molecules because this transition is experimentally observed for the GaAs molecule in the gas phase. After the inclusion of the spin−orbit interaction, the nature of the potential energy curves changes due to avoided crossings. The $A^3\Pi_{0^+}$ component is the only one that survives the predissociation. This component undergoes six possible transitions, which are listed in Table 5. The calculations suggest that the $A^3\Pi_{0^+}-X^3\Sigma_1^-$ transition is the strongest among all. Transition dipole moment functions of all six transitions are shown in Figure 3c. In the Franck−Condon region, the transition moments of the $A^3\Pi_{0^+}-X^3\Sigma_1^-$ transition show a broad maximum, and the values are much larger compared to those of $A^3\Pi_{0^+}-X^3\Sigma_{0^+}^-$. Therefore, the former transition is found to be comparatively strong. It may be noted that the $A^3\Pi_{0^+}-{}^3\Pi_{0^+}$ transition has also very high transition moments. But the smaller Franck−Condon overlap terms due to the shorter r_e of the upper state as compared with the lower state reduce the transition probabilities to some extent. The remaining transitions from the $A^3\Pi_{0^+}$ state are found to be considerably weak. After adding transition probabilities of all possible transitions, the radiative lifetime of the $A^3\Pi_{0^+}$ component at $v'=0$ is estimated to be 436 ns.

Comparison with InP and InSb Molecules. The electronic structure and spectroscopic properties of group III−V diatomic molecules are found to be very similar. In the present context it would be relevant to compare the properties of InAs obtained in the present study with those of InP and InSb molecules studied recently[23,25] at the same level of MRDCI calculations. These molecules have identical ground states of the $X^3\Sigma^-$ symmetry. As expected, the ground-state r_e of InAs falls between r_e(InP) and r_e(InSb). The equilibrium vibrational frequencies are also in the expected order ω_e(InP) > ω_e(InAs) > ω_e(InSb). The ground-state D_e of InP and InAs are comparable, while for the heavier InSb molecule the dissociation energy is larger by 0.1 eV. The first excited state ($^3\Pi$), described by the $...\sigma'\pi^3$ configuration, has a greater stability than the closed-shell $^1\Sigma^+$ state. This is true for all three molecules compared here. However, such a stability is found to be largest for InP, which has a greater $^1\Sigma^+-{}^3\Pi$ energy separation. The equilibrium bond lengths of the $^3\Pi$ state of InX (X = P, As, Sb) are shorter than the corresponding ground-state r_e by about 0.2 Å. This is generally true for all group III−V diatomic molecules because of the greater stability of the σ' MO compared with π MO. The transition energy of the $^3\Pi$ state of InAs is somewhat smaller than that expected from the corresponding energies for InP and InSb molecules. The $^1\Pi-{}^3\Pi$ energy separation for InP and InAs are of comparable magnitudes, while for InSb the splitting is found to be somewhat smaller. Similar results have been noted for the gallium series of molecules.

The interaction between $^1\Sigma^+$ and $2^1\Sigma^+$ states looks very similar for all three molecules and it leads to an avoided crossing around 5 a_0, whereas a sufficient energy-gap between $2^1\Sigma^+$ and $3^1\Sigma^+$ prevents them to mix. On the other hand, third and fourth $^1\Sigma^+$ states interact considerably near 5.5 a_0 because of the small energy difference. The calculations show that such interaction increases with the mass of the molecule. As a result, the avoided crossing between $3^1\Sigma^+$ and $4^1\Sigma^+$state curves is found to be strongest in InSb. For all diatomic molecules of group III−V, the $4^1\Sigma^+$ state is found to be strongly bound. At the same level of calculation, transition energies of the $4^1\Sigma^+$states lie in the region of 31 500−32 500 cm^{-1}. However, the existence of this state is not yet known for any of group III−V molecules.

The $2^3\Pi$ states of three molecules compared here show shallow long-distant potential minima, which arise because of their strong interactions with the lowest $^3\Pi$ states. The characteristics of the $3^3\Pi$ state which is designated as A, are similar for these indium series of molecules. Although no experimental results are available yet, the $A^3\Pi-X^3\Sigma^-$ transitions of all three molecules should be observed in the 20 000−22 000 cm^{-1} range, with the smaller value for the heavier InSb as expected. The MRDCI calculations show that the A−X transitions for these molecules are considerably strong. The computed

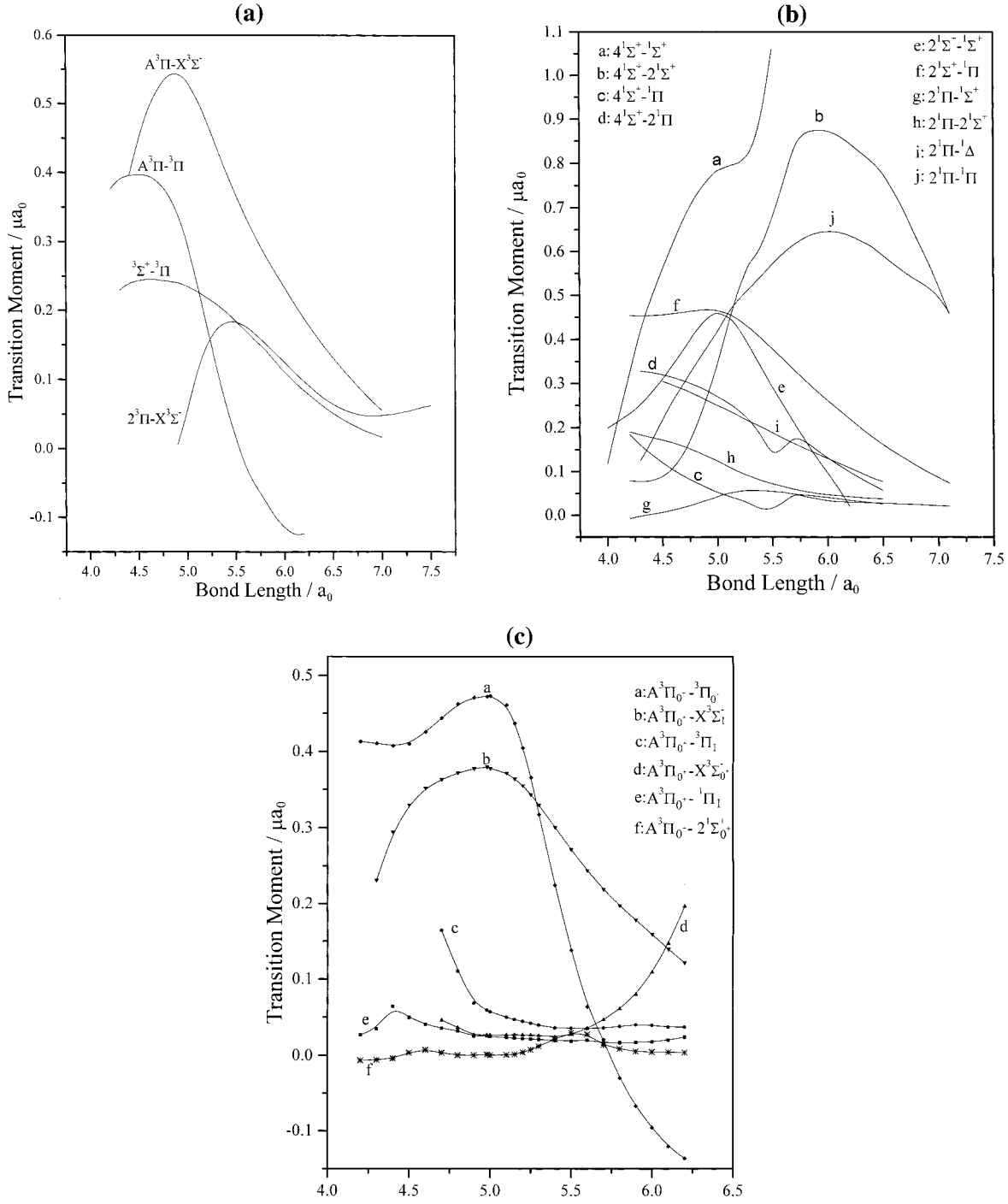

Figure 3. (a) Transition moments of some triplet−triplet transitions as a function of the bond length. (b) Transition moments of some singlet−singlet transitions as a function of the bond length. (c) Transition moments of six transitions from $A^3\Pi_{0^+}$.

TABLE 5: Radiative Lifetimes of the $A^3\Pi_{0^+}$ Component of InAs at ($v' = 0$)[a]

transition	partial lifetimes(s) of $A^3\Pi_{0^+}$
$A^3\Pi_{0^+}-X^3\Sigma_1^-$	6.05(−7)
$A\ ^1\Pi_{0^+}-^3\Pi_{0^+}$	1.60(−6)
$A^3\Pi_{0^+}-X\ ^3\Sigma_{0^+}^-$	7.42(−5)
$A^3\Pi_{0^+}-^1\Pi_1$	7.87(−4)
$A^3\Pi_{0^+}-2\ ^1\Sigma_{0^+}^+$	6.72(−3)
$A^3\Pi_{0^+}-^3\Pi_1$	6.29(−1)
Total lifetime(s) of $A^3\Pi_{0^+}$	$\tau(A^3\Pi_{0^+}) = 4.36(-7)$

[a] Values in the parentheses are the powers to the base 10.

radiative lifetimes of the $A^3\Pi$ state for InP, InAs, and InSb are 190, 249, and 530 ns, respectively. The repulsive curve of $^5\Sigma^-$ crosses the potential energy curves of $2^3\Pi$ and $A^3\Pi$ in a similar manner for all three molecules. In the presence of the spin−orbit coupling, the position of this crossing plays an important role in determining the transitions from the spin−orbit components of the $A^3\Pi$ state. The components with $\Omega = 2$, 1, and 0^- of $^5\Sigma^-$ and $^3\Pi$ states interact strongly in a similar way for InP, InAs, and InSb molecules. This has resulted predissociations of these components, whereas only the 0^+ components of $2^3\Pi$ and $A^3\Pi$ survive the predissociations. Therefore, the $A^3\Pi_{0^+}-X^3\Sigma_{0^+}^-$ transition should be observed for all these molecules. At the MRDCI level of calculation, the total estimated lifetimes of the $A^3\Pi_{0^+}$ component at $v' = 0$ for InP and InAs molecules are comparable, while for InSb, this component is longer lived.

IV. Conclusion

Ab initio based MRDCI calculations using RECPs and suitable Gaussian basis sets determine an accurate picture of the electronic spectrum of the indium arsenide molecule. There are at least 18 $\Lambda-S$ states which are bound within 40 000 cm^{-1}. Like any other isovalent group III−V molecule, InAs has a ground state of the $X^3\Sigma^-$ symmetry. The computed ground-state r_e and ω_e are 2.76 Å and 179 cm^{-1}, respectively. The only known experimental ω_e of 180.6 cm^{-1} agrees almost exactly with the calculated value. However, the present treatment is known to overestimate r_e and underestimate ω_e. Although no experimental bond length is available at present, it is expected that the observed r_e of InAs in the ground state would be somewhat less than 2.76 Å. The calculated transition energy of the first excited state ($^3\Pi$) is considerably lower than the observed value reported in argon matrices at low temperature. The ground-state dissociation energy of InAs computed from the MRDCI treatment is 1.31 eV. The value is expected to be underestimated because of the use of effective core potentials and the neglect of d-correlation for both In and As atoms in the CI steps. However, no experimental D_0^0 value for InAs has been reported so far. The $A^3\Pi$ state in the region of 21 000 cm^{-1} is important for its transition to the ground state. The present calculations also predict that the $A^3\Pi-X^3\Sigma^-$ transition is highly probable. The computed radiative lifetime of the $A^3\Pi$ state after adding all possible transition probabilities is about 249 ns. Among other dipole-allowed transitions, $2^3\Sigma^+(II)-^3\Pi$ and $4^1\Sigma^+-^1\Sigma^+$ transitions are found to be strong. In fact, the $4^1\Sigma^+-^1\Sigma^+$ transition has the largest calculated transition probabilities, and the estimated lifetime of the $4^1\Sigma^+$ state at $\upsilon' = 0$ is only 66 ns. Two low-lying quintets such as $^5\Pi$ and $^5\Sigma^-$ are repulsive, while several high-lying quintet states above 33 000 cm^{-1} are found to be bound. The spin−orbit coupling introduced to interact with 22 Λ-S states reveals the ground-state zero-field splitting of 92 cm^{-1} InAs as compared with the observed value of 119 cm^{-1}. The $X^3\Sigma_{0^+}$ component is lying lower that the other component with $\Omega = 1$. The maximum spin−orbit splitting in the spectroscopically inverted $^3\Pi$ state is about 1200 cm^{-1}. Three Ω components, 2, 1, and 0^-, of $A^3\Pi$ undergo predissociations because of their interactions with the corresponding components of the repulsive $^5\Sigma^-$ state. The $A^3\Pi_{0^+}$ component which survives the predissociation should undergo the strongest $A^3\Pi_{0^+}-X^3\Sigma_1$ transition, while the transition to the other component such as $A^3\Pi_{0^+}-X^3\Sigma_{0^+}$ is comparatively weak. At the lowest vibrational level, the $A^3\Pi_{0^+}$ component has a lifetime of about 436 ns.

Acknowledgment. The authors sincerely thank Professor Dr. Robert J. Buenker, Wuppertal, Germany for giving the permission to use his MRDCI program packages. One of us (D.G.) is thankful to the CSIR, India for the award of Junior Research Fellowship.

References and Notes

(1) O'Brien, S. C.; Liu, Y.; Zhang, Q.; Heath, J. R.; Tittel, F. K.; Curl, R. F.; Smalley, R. E. *J. Chem. Phys.* **1986**, *84*, 4074.
(2) Liu, Y.; Zhang, Q.; Tittel, F. K.; Curl, R. F.; Smalley, R. E. *J. Chem. Phys.* **1986**, *85*, 7434.
(3) Zhang, Q.; Liu, Y.; Curl, R. F.; Tittel, F. K.; Smalley, R. E. *J. Chem. Phys.* **1988**, *88*, 1670.
(4) Wang, L.; Chibante, L. P. F.; Tittel, F. K.; Curl, R. F.; Smalley, R. E. *Chem. Phys. Lett.* **1990**, *172*, 335.
(5) Jin, C.; Taylor, K.; Conciecao, J.; Smalley, R. E. *Chem. Phys. Lett.* **1990**, *175*, 17.
(6) Lou, L.; Wang, L.; Chibante, L. P. F.; Laaksonen, R. T.; Nordlanden, P.; Smalley, R. E. *J. Chem. Phys.* **1991**, *94*, 8015.
(7) Lemire, G. W.; Bishea, G. A.; Heidecke, S. A.; Morse, M. D. *J. Chem. Phys.* **1990**, *92*, 121.
(8) Cowley, A. H.; Jones, R. A. *Angew. Chem., Int. Ed. Engl.* **1989**, *28*, 1208.
(9) Arnold, C. C.; Neumark, D. M. *J. Chem. Phys.* **1994**, *99*, 3353.
(10) Arnold, C. C.; Neumark, D. M. *J. Chem. Phys.* **1994**, *100*, 1797.
(11) Xu, C.; deBeer, E.; Arnold, D. W.; Arnold, C. C.; Neumark, D. M. *J. Chem. Phys.* **1994**, *101*, 5406.
(12) Arnold, C. C.; Neumark, D. M. *Can. J. Phys.* **1994**, *72*, 1322.
(13) Burton, G. R.; Xu, C.; Arnold, C. C.; Neumark, D. M. *J. Chem. Phys.* **1996**, *104*, 2757.
(14) Li, S.; Van Zee, R. J.; Weltner, W., Jr. *J. Phys. Chem.* **1994**, *98*, 2275.
(15) Li, S.; Van Zee, R. J.; Weltner, W., Jr. *J. Phys. Chem.* **1993**, *97*, 11393.
(16) Balasubramanian, K. *Relativistic Effects in Chemistry Part A. Theory and Techniques*; Wiley-Interscience: New York, 1997.
(17) Balasubramanian, K. *Relativistic Effects in Chemistry Part B. Applications to Molecules and Clusters*; Wiley-Interscience, New York, 1997.
(18) Feng, P. Y.; Balasubramanian, K. *Chem. Phys. Lett.* **1998**, *283*, 167.
(19) Feng, P. Y.; Balasubramanian, K. *Chem. Phys. Lett.* **1998**, *284*, 313.
(20) Feng, P. Y.; Balasubramanian, K. *Chem. Phys. Lett.* **1997**, *265*, 41.
(21) Feng, P. Y.; Balasubramanian, K. *Chem. Phys. Lett.* **1997**, *265*, 547.
(22) Manna, B.; Das, K. K. *J. Mol. Struct.* (*THEOCHEM*) **1999**, *467*, 135.
(23) Manna, B.; Dutta, A.; Das, K. K. *J. Phys. Chem.* **2000**, *A 104*, 2764.
(24) Manna, B.; Das, K. K. *J. Phys. Chem.* **1998**, *A 102*, 9876.
(25) Manna, B.; Dutta, A.; Das, K. K. *J. Mol. Struct. (THEOCHEM)* **2000**, *497*, 123.
(26) Dutta, A.; Chattopadhyay, A.; Das, K. K. *J. Phys. Chem. A* **2000**, *104*, 9777.
(27) Balasubramanian, K. *J. Chem. Phys.* **1987**, *86*, 3410; Erratum: *J. Chem. Phys.* **1990**, *92*, 2123.
(28) Balasubramanian, K. *Chem. Rev.* **1990**, *90*, 93.
(29) Balasubramanian, K. *J. Mol. Spectrosc.* **1990**, *139*, 405.
(30) Meier, U.; Peyerimhoff, S. D.; Bruna, P. J.; Karna, S. P.; Grein, F. *Chem. Phys.* **1989**, *130*, 31.
(31) Toscano, M.; Russo, N. *Z. Physica D* **1992**, *22*, 683.
(32) Musolino, V.; Toscano, M.; Russo, N. *J. Comput. Chem.* **1990**, *11*, 924.
(33) Oranges, T.; Musolino, V.; Toscano, M.; Russo, N. *Z. Physica D* **1990**, *17*, 133.
(34) LaJohn, L. A.; Christiansen, P. A.; Ross, R. B.; Atashroo, T.; Ermler, W. C. *J. Chem. Phys.* **1987**, *87*, 2812.
(35) Hurley, M. M.; Pacios, L. F.; Christiansen, P. A.; Ross, R. B.; Ermler, W. C. *J. Chem. Phys.* **1986** *84*, 6840.
(36) Balasubramanian, K. *J. Chem. Phys.* **1990**, *93*, 507.
(37) Alekseyev, A. B.; Liebermann, H.-P.; Hirsch, G.; Buenker, R. J. *J. Chem. Phys.* **1998**, *108*, 2028.
(38) Buenker, R. J.; Peyerimhoff, S. D. *Theor. Chim. Acta* **1974**, *35*, 33.
(39) Buenker, R. J.; Peyerimhoff, S. D. *Theor. Chim. Acta* **1975**, *39*, 217.
(40) Buenker, R. J. *Int. J. Quantum Chem.* **1986**, *29*, 435.
(41) Buenker, R. J.; Peyerimhoff, S. D.; Butcher, W. *Mol. Phys.* **1978**, *35*, 771.
(42) Buenker, R. J. In *Proceedings of the Workshop on Quantum Chemistry and Molecular Physics;* Burton, P., Ed.; University Wollongong: Wollongong, Australia; 1980. *Studies in Physical and Theoretical Chemistry*; Carbó, R., Ed.; Elsevier: Amsterdam, 1981; Vol. 21 (Current Aspects of Quantum Chemistry).
(43) Buenker, R. J.; Phillips, R. A. *J. Mol. Struct.* (*THEOCHEM*) **1985**, *123*, 291.
(44) Davidson, E. R. In *The World of Quantum Chemistry*; Daudel, R.; Pullman, B., Ed.; Reidel: Dordrecht, 1974.
(45) Hirsch, G.; Bruna, P. J.; Peyerimhoff, S. D.; Buenker, R. J. *Chem. Phys. Lett.* **1977**, *52*, 442.
(46) Cooley, J. W. *Math. Comput.* **1961**, *15*, 363.
(47) Moore, C. E. *Atomic Energy Levels*; National Bureau of Standards: Washington, DC; Vol 3.